Advanced Steel Construction – Vol. 16 No.1 (2020) 37–46
DOI:10.18057/IJASC.2020.16.1.5

INFLUENCE OF THE CORE-RESTRAINER CLEARANCE ON THE MECHANICAL PERFORMANCE OF SANDWICH BUCKLING-RESTRAINED BRACES

Lu-qi Xie [1], Jing Wu [1, *], Jian-hua Shi [2] and Yun-qing Zhu [1]

[1] *The Key Laboratory on Concrete and Prestressed Concrete Structures of Ministry of Education, Southeast University, Nanjing, China*

[2] *Nanjing Jiangbei New Area Center Development Co. Ltd, Nanjing, China*

** (Corresponding author: E-mail: seuwj@seu.edu.cn)*

ABSTRACT

The out-of-plate clearance between the core member and the restrainer is an important parameter for evaluating the hysteretic performance of a buckling-restrained brace (BRB) and may make a significant impact on its low-cycle fatigue capacity via the friction value of the core member under compression. A theoretical derivation and finite element analysis are conducted on BRBs with various clearances, in which the distribution of the friction and axial strain along the core member is obtained. The results reveal that the contact force between the core member and the restrainer under compression increases with the clearance, leading to increased friction on the contact area of the core member and a nonuniform strain distribution along the core member. Moreover, an experimental study of 8 "sandwich" BRB specimens with different clearances was conducted. The test results indicate that the compression-strength adjustment factor of the BRBs increases with the clearance; moreover, the maximum cycle number under large axial strain is significantly decreased, indicating a lower energy dissipation capacity. Additionally, a higher stiffness demand of the restrainer is needed for an excessively large clearance, which leads to a poor cost performance. In conclusion, a threshold value for the core-restrainer clearance should be proposed, and a determination method is suggested via a formula derivation at the end of this paper.

ARTICLE HISTORY

Received: 12 March 2019
Revised: 8 October 2019
Accepted: 11 October 2019

KEYWORDS

Buckling-restrained brace;
clearance;
compression-strength adjustment factor;
multi-wave buckling;
low-cycle fatigue property

1. Introduction

A buckling-restrained brace (BRB, shown in Fig. 1) is extensively employed as a lateral-resisting member and damper in newly built structures and the reconstruction of existing structures; BRBs are regarded as an effective method for performance-based seismic design (Usami et al. [1], Tsai et al. [2], Chou et al. [3], Vargas et al. [4]). BRBs can yield in tension and compression without buckling, and they exhibit stable elasto-plastic hysteretic behavior and dissipate energy during strong earthquakes (Tsai et al. [2], Chou et al. [3]). The main structural members remain elastic under strong ground motions when BRBs yield, which can ensure a stable integrality and robustness of the whole structure. The seismic rehabilitation of a structure can be achieved by replacing the BRBs, which is convenient for implementation (Usami et al. [5], Feng et al. [6]). The core member of a BRB may buckle along the weak axis under compression, while the buckling trend is prevented by the restrainer, and multi-wave buckling is sequentially formed in compression (Wu et al. [7], Takeuchi et al. [8]). The multi-wave buckling of a core member enables contact between the core member and the restrainer and produces friction between them, which does not exist in the tensile condition. The existence of friction in compression may cause a nonidentity regarding the compression and tensile strength, which can be evaluated as the compression-strength adjustment factor β, as expressed by Eq. (1):

$$\beta = \max\left(\frac{P_{\max}^{i}}{T_{\max}^{i}}\right) \tag{1}$$

where $P_{\max}{}^{i}$ and $T_{\max}{}^{i}$ are the amplitude of the axial compression force and the amplitude of the tensile force, respectively, in the ith cycle of the BRB. The friction may generate a nonuniform distribution of axial strain along the core member. Thus, some local parts of the core member may undergo strain concentration, which causes a decrease in the low-cycle fatigue capacity of BRBs. A larger β value indicates an amplified imbalance of the tensile and compressive capacity with a considerable strain concentration. AISC 340-10 [9] stipulates that the value of β should not exceed 1.3. A method for restricting the β value is to lay unbonded material on the surface of the core member (Uang et al. [10]), setting stoppers on the middle section of the core member (Xie et al. [11]) and controlling the clearance between the core member and the restrainer (Wu et al. [7]). Wu et al. [7] conducted a formula derivation and proposed that the variation of clearance between the core member and the restrainer will affect the magnitude and the distribution of friction force. The friction increases with the clearance, which causes an increase in the compression force and the β value. Jiang et al. [12] theoretically and numerically analyzed the stress state of the assembled buckling-restrained braces (ABRBs) under compression. The stress state under single-wave buckling and multi-wave buckling was obtained, while the design method on the pinned ABRB with a flat core was also proposed. Wu et al. [13] theoretically and experimentally investigated the buckling mechanism of the steel cores of BRBs, in which formulas for the maximum contact force and maximum bending moment of the restrainer were proposed.

Fig. 1 BRBs in a frame

The cumulative plastic deformation (CPD) capacity is an essential performance demand criterion for evaluating the energy dissipation capacity of BRBs (FEMA450 [14]), which is expressed as

$$CPD = \sum \left|\Delta\varepsilon_{pi}\right| / \varepsilon_{y} \tag{2}$$

where $\Delta\varepsilon_{\mathrm{pi}}$ is the plastic strain amplitude in the ith cycle and ε_{y} is the yielding strain of the core member.

Researchers have conducted a series of studies regarding the CPD capacity of BRBs. Black et al. [15] experimentally investigated the CPD regulation of BRBs with various loading histories. Wang [16], Jia [17] and Guo [18, 19] researched the BRBs manufactured using different materials and constructions via constant-amplitude and variable-amplitude cyclic loading, respectively, and simultaneously conducted intensive studies regarding the CPD capacity of BRBs on the component level. The research results reveal that the CPD capacity is closely related to the fabrication method and loading history of the BRBs. Researchers have also computationally and experimentally explored BRB frames (BRBFs) and revealed the seismic demand of the CPD capacity of BRBs during strong earthquakes. Sabelli [20] proposed a minimum demand of 185 based on time history analyses of a three-story BRBF and a six-story BRBF.

Iwata et al. [21] suggested a minimum CPD capacity of 292, while Usami et al. [22] proposed a minimum CPD capacity of 400. ANSI/AISC [9] stipulates a minimum CPD capacity of the BRB of 200 to ensure the requirement of low-cycle fatigue capacity. Lin et al. [23] proposed the seismic design method of thin profile core members. Matsui et al. [24] also studied the cumulative deformation capacity of BRBs by considering local buckling of the core plates. As the strain distribution on the axial direction of a BRB is nonuniform under compression due to the existence of friction, the strain concentration may cause a decrease in the CPD capacity of the BRB. Thus, the clearance between the core member and the restrainer is a key parameter in evaluating the CPD capacity of BRBs.

A finite element analysis and experimental study are conducted on "sandwich" BRBs to quantitatively analyze the influence of the clearance on the deformation and energy dissipation capacity of BRBs. A simplified model of "sandwich" BRBs was developed, and 6 different clearance values were chosen for the parametric analysis. Eight "sandwich" BRBs with different clearance values were manufactured for the experimental study. The friction distributions on the core member and the restrainer are obtained. The axial strain distribution and the compression-strength adjustment factor of the BRBs are also extracted via the computational and the experimental analysis, respectively. The variation in the low-cycle fatigue performance of BRBs with different clearance values and the deformation or buckling of the core members are further analyzed.

2. Theoretical and numerical analyses of brbs with different clearance values

2.1. Theoretical analysis

2.1.1 Contact force and friction between the core member and restrainer

According to Reference [7], the core member of a BRB buckles into a multi-wave shape under axial compression. The quantity of the waves increases with the axial compression load, while the "point contact situation" and "line-contact situation" alternatively appear, which causes increases in the contact point number and contact force. The contact force T_0 of one contact point in the multi-wave buckling condition is given as

$$T_0 = \frac{Py_0}{\pi}\sqrt{\frac{P}{EI}} \tag{3}$$

where P is the axial force of the core member, y_0 is the clearance between the core member and the restrainer, E is the Young's modulus, and I is the moment of inertia of the core member.

As shown in Eq. (3), the contact force T_0 is proportional to y_0 for a certain P. Once the core member yields, E should be replaced with E_t, which is the tangent modulus of the steel (Takeuchi and Wada [25]).

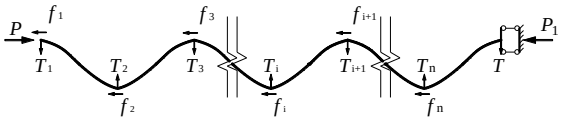

Fig. 2 Force distribution of the half core member along the length direction

With the relative movement between the core member and the restrainer, friction is produced and continuously increases with increasing axial compression load. The distribution of friction along the axial direction of the core member is also closely related to the wave shape, as shown in Fig. 2. A "relative fixed point" exists between the two members, which can balance the friction on the two sides of the core member if the point is set in the core middle. A stopper is usually set as the relative fixed point. The friction magnitude of the core member on one side of the stoppers can be expressed as

$$f = \mu\sum_{i=1}^{n} T_i \tag{4}$$

where f is the summary of the friction on the semistructure of the core member, μ is the friction coefficient between the core and the restrainer, and T_i is the contact force of the i^{th} wave (i=1, 2, …n) along the core member, in which the number of waves on one side of the core member can be expressed as

$$n = \frac{1}{4}\sqrt{\frac{P}{P_E}} \tag{5}$$

where P_E is the Euler critical buckling force or the postyield critical buckling force of the core member.

As shown in Figure 2, the axial force along the core member longitude is different due to the existence of friction. The axial force decreases with the position drawing near the stopper, which can be expressed as:

$$P_1 = P - \sum_{i=1}^{n} f_i \tag{6}$$

The friction also increases with the amplification of the clearance and decreases with the amplification of the flexural rigidity. Furthermore, the magnitude of the axial compression load determines the quantity of the waves, the wavelength and the friction magnitude in one wave. Thus, the magnitude and distribution of friction on the core member can be obtained via the iteration method. In this paper, the lengths of the buckling waves on the core member are assumed to be equal, which indicates that the friction in each wave is equal.

2.1.2 Influence of friction on the compression-strength adjust factor

The existence of the compression-strength adjust factor β may cause the yielding force to exceed the expected range, which may produce an uncertainty in the design. However, the friction is an important factor that affects the β value, although it is not a unique factor.

According to Eq. (3) and (4), the friction between the core member and the restrainer members also increases with the clearance, which may cause a larger β value. AISC 340-10 [9] stipulates that the β value should not exceed 1.3; the threshold value range of the clearance should be limited to a certain BRB. In this paper, the index β of the test specimens can be obtained by the hysteretic curves that are gathered from the force transducer on the test machines and the linear variable differential transducers (LVDTs).

2.1.3 Influence of friction on the core member axial strain

The existence of friction will cause a nonuniform axial force and strain distribution along the length of the core member according to Eq. (4) and (6), while the axial strain decreases from the end of the core member to the middle of the core member due to the force distribution. Furthermore, as the BRB commonly functions the under cyclic load of tension and compression during strong earthquakes, the strain distribution of a core member in tension should also be considered. When the core member develops into tension from compression, the contact between the core member and the restrainer is relieved because the buckling of the core member is rehabilitated. The friction is also relieved, while the axial force along the core member is equal. Because the section area along the core member length in compression is different and the area of the core member at the end is larger than that in the middle, the axial stress in the core member in the middle is larger than that at the end, which indicates that the strain distribution along the core member is not uniform, even if a further nonuniform level is attained. This phenomenon reveals that the no uniform distribution of the strain along the length direction of the core member will become increasingly important during the cyclic load of tension and compression. After the core member yields, the stiffness will significantly decrease, and even a slight increase in the stress will cause a large strain variation. In this case, the nonuniform distribution of the strain in a core member is substantially more serious, as shown in Fig. 3. Once the core member yields and the stiffness decreases, the quantity of the buckling waves increases, which indicates that the quantity of the contact points and the friction significantly increase, and the strain concentration will become even

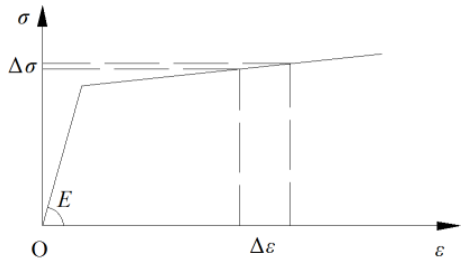

Fig. 3 Stress-strain relationship of the core member material

more important. As the low-cycle fatigue performance of a BRB decreases with increasing strain amplitude, the strain concentration of a core member should be avoided. As shown in Eq. (3) and (4), controlling the clearance between the core member and the restrainer can be an effective method.

2.2. Numerical model verification

The theoretical analysis of the influence of clearance listed in Section 2.1 is verified in this section by a finite element method. A simplified analytical model of BRBs is established in ABAQUS/Explicit, in which the restrainer is regarded as rigid, while the material nonlinearity, geometric nonlinearity and contact nonlinearity are comprehensively considered. The core member of a BRB is simplified as a steel plate, which disregards the influence of the connection details between the BRB and the structural members. Both the core member and the restrainer are modeled with S4R elements. An axial load is applied to both ends of the core member, while a fixed constraint is applied to the middle. Additionally, the fixed constraints are also applied to the restrainers for simulating the rigid plates. The clearance is the key parameter that is varied; values of 0.5 mm, 1 mm, 1.5 mm, 2 mm, 2.5 mm and 3 mm are selected in this paper. To determine the effect of the out-of-plane clearance on BRBs, the in-plane deformation is disregarded when establishing the model. Because the stoppers settling in the middle of the core member may affect the friction distribution of the BRB, the load is applied to both ends of the core member, while the middle is restrained. A bilinear kinematic hardening model is selected as the constitutive relationship, in which the yielding strength (σ_s) is 296 MPa, as obtained from material property tests. The Young's modulus is 2.037×10^5 N/mm^2, while the tangent modulus is 4840 N/mm^2. The Poisson's ratio is 0.3. The parameters of the models are listed in Table 1 below.

Table 1
Model parameters

Model No.	CL (mm)	CW (mm)	RL (mm)	RW (mm)	CR(y_0) (mm)	LA (mm)
1	1075	100	1150	200	0.5	32.25
2	1075	100	1150	200	1	32.25
3	1075	100	1150	200	1.5	32.25
4	1075	100	1150	200	2	32.25
5	1075	100	1150	200	2.5	32.25
6	1075	100	1150	200	3	32.25

Note: CL stands for the core member length; CW stands for the core member width; RL stands for the restrainer length; RW stands for the restrainer width; CR stands for the clearance between the core member and restrainer; LA is the loading amplitude of the model.

Finite element analyses are conducted on all six models listed in Table 1, in which the loading protocol is one cyclic loading on a 3% nominal strain amplitude in tension and compression. The conditions of considering friction and not considering friction are applied. Analyses that disregard the influence of friction are used to verify the multi-wave buckling theory mentioned in Section 2.1, while analyses that consider the friction coefficient are conducted to analyze the nonuniform distribution extent of strain along the core member for different clearance magnitudes.

Fig. 4 Multi-wave buckling of the core member (Model 1; the deformation scaling factor is 10)

First, friction is disregarded. The buckling characteristic of Model 1 under the maximum compression load is shown in Fig. 4. The core member is settled in the line-contact condition. The shapes of the buckling segments are similar, while the distribution of the line-contact length is nonuniform. The distribution of the line-contact length is random, which does not have an effect on the validity of the theory mentioned in Section 2.1.

The contact force T of the six BRB core members can be obtained using Eq. (3), while the finite element analysis results of the contact force T are also obtained. The results of the ratio between the finite element analysis results and the theoretical values are listed in Fig. 5, in which the horizontal axial represents the theoretical values, while the vertical axial represents the finite element analyses results. The results reveal that the ratio values primarily distribute around the 45° line, which indicates that the results obtained from the two methods coincide. The increase in the contact force T with increasing clearance, which coincides with the theory mentioned in Section 2.1, is confirmed.

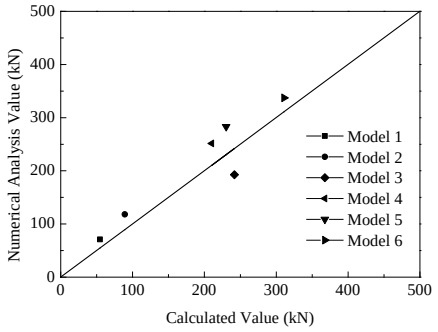

Fig. 5 Contact force of models

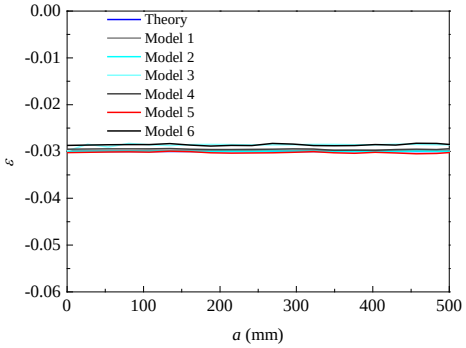

Fig. 6 Strain distribution of 6 models without friction under maximum deformation (semi-structure on the left)

Fig. 6 lists the axial strain distribution of the core member in the models, which disregards the effect of friction. The strain distribution along the axial direction is consistent, which is a nearly 3% constant amplitude under the maximum deformation.

Second, to consider friction, a friction factor of 0.3 is added to the models. The results reveal that the friction distribution is contrary between the left part of the core member and the right part of the core member, in which the middle of the core member is restrained while the load is symmetrically applied to both ends. The direction of the friction on the restrainer is opposite that on the core member, which is consistent with the interaction principle of forces.

The sum of the absolute values of friction along the core member length direction is chosen as the index for evaluating the effect of friction on the core member performance. The relationship between the friction value and the loading history of the six models is shown in Fig. 7. No contact occurs between the core member and the restrainer when the specimens are in tension, which causes zero friction. Once the BRB is under compression and the load exceeds the critical buckling force, the core member starts to buckle and make contact with the restrainer. The friction increases from the initial contact to the largest compression deformation amplitude and then maintains the maximum value. The friction decreases with the unloading of the compression load, while a reverse friction appears, which is due to the relative movement trend between the core member and the restrainer in the unloading stage contrary to the loading stage. The core member will be separated from the restrainer with further unloading, which indicates that the friction decreases to zero.

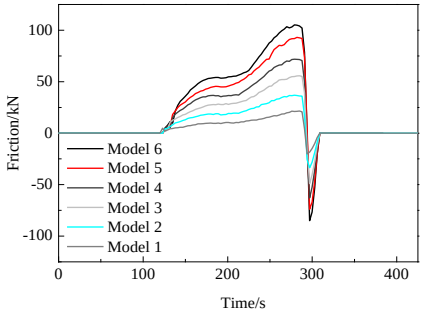

Fig. 7 Friction history

The nonuniform axial strain distribution is shown in Fig. 8, which is consistent with the previously mentioned theoretical derivation. The axial

force of the ends of the core member is greater than that in the middle, with a continuous decreasing trend along the length direction that is symmetric with the intermediate boundary, which can verify the accuracy of Eq. (6).

A comparison of Fig. 8 with Fig. 6 indicates that the friction is an immediate factor of the nonuniform strain distribution. The strain distributions also indicate that strain near the end of the core member with a nominal amplitude of 3% is considerably greater than 3%, which may cause a decrease in the low-cycle fatigue performance. This conclusion is consistent with the theoretical analysis in Section 2.1.3. Furthermore, fracture of the BRB is predicted to occur on one end of the core member.

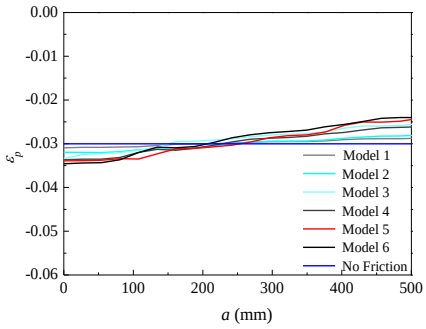

Fig. 8 Strain distribution of 6 models under a deformation amplitude of 3% (semi-structure on the left)

3. Experimental study of BRBs with various clearance values

3.1. Main sections

3.1.1 Axial tension test

The BRBs should be manufactured of steel with a high ductility performance, which can undergo a large deformation amplitude and a reverse loading test without fracturing. In this paper, Q235 steel is selected, and the mechanical properties are obtained from the axial tension test, including the yield strength, yield ratio, and percentage elongation, as reported in Table 2.

Table 2
Test results of axial tension test

No.	σ_y (MPa)	σ_p (MPa)	σ_y/σ_p (%)	E_s (N/mm^2)	μ (%)
1	276.0	420.0	65.7	205000	38.7
2	282.0	423.0	66.7	204000	39.6
3	283.0	432.0	65.5	205000	41.9
Average	280.3	425.0	66.0	204700	40.1

Note: σ_y stands for the yielding strength; σ_p stands for the limit strength; σ_y/σ_p is the yield ratio of the specimen; E_s is the Young's modulus; μ stands for the percentage elongation.

3.1.2 Low-cycle fatigue performance of Q235 steel

The low-cycle fatigue property of the BRBs substantially depends on the fatigue capacity of the steel, which is commonly related to its elasto-plastic performance. In this paper, the low-cycle fatigue properties of the selected Q235 steel are chosen based on the test results presented in Reference [11], as listed in Table 3.

Table 3
Test results of material experiments

No.	ε_a	N_f	N_{fave}
1	0.01	276	378
2	0.01	481	
3	0.02	104	104
4	0.02	104	
5	0.03	19	19
6	0.03	19	

Note: ε_a is the strain amplitude of the specimen; N_f is the number of failure cycles; N_{fave} is the average value of N_f.

Table 3 indicates that the low-cycle fatigue property of the specimens significantly decreases with increasing strain amplitude. Once the strain amplitude exceeds 2%, the low-cycle fatigue property decreases even more rapidly. However, the strain amplitude of the BRBs usually exceeds 2% during rare earthquakes. Thus, the study of the low-cycle fatigue property of BRBs is essential, especially when considering the clearance.

3.2. Design of the BRB specimens

In this paper, a type of all-steel sandwich BRB is chosen for experimental study of the influence of clearance on the mechanical property and low-cycle fatigue performance of BRBs. The clearance of the sandwich BRBs can be easily controlled, and the construction of the BRBs is convenient (Usami et al. [5]).

A sandwich BRB is composed of a core plate, a restrainer and unbonded material, as shown in Fig. 9. The core plate is a steel plate with an expanded section segment on the ends, while stiffening ribs are welded to the end of the core member, forming a cross-section. The restrainer is composed of two restraining plates and two filler strips that are connected by high-strength bolts to form a square socket, which can effectively restrain the buckling of the core member. Grooves are set on the end of the restraining plates to avoid contact between the restraining plates and the stiffening ribs when the specimen is under compression. The restraining plates should remain elastic and enable a sufficient amount of out-of-plane stiffness to resist the contact force between the core member and the restrainer without overall buckling of the BRB. This demand can be obtained by thickening the restraining plate or welding stiffening ribs on the back of the restraining plate.

The key factor in this study is the clearance in the out-of-plane direction, which can be adjusted by changing the thickness of the filler strips or adding some thin steel slices between the restraining plate and the filler strip. The dimensions of the core plate, restraining plates and filler strips are listed in Fig. 10. The clearance value d is selected to be 1.0 mm, 1.5 mm and 2.0 mm. In this paper, a total of 8 specimens were analyzed. The factors chosen for research are the key factor clearance and the thickness of the restraining plate. The main geometric factors of the specimens are listed in Table 4. The specimens are named "BRB-clearance-strain amplitude", and BRB-1-2 indicates that the specimen is set with a clearance of 1 mm and a loading strain amplitude of 2%.

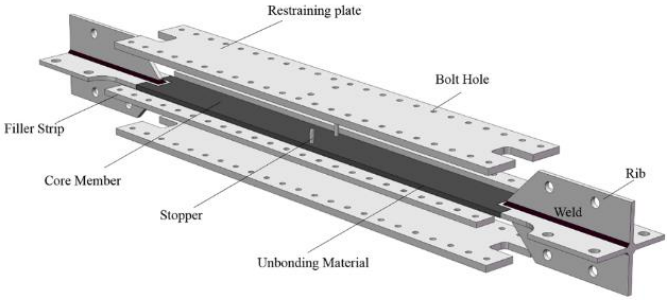

Fig. 9 Construction of a sandwich BRB

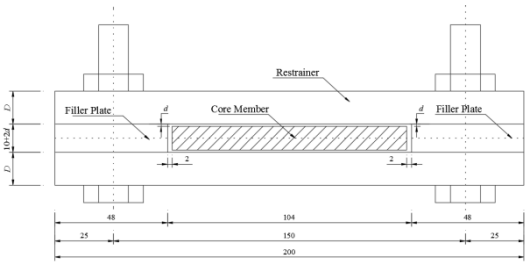

(a) Cross-section of BRB

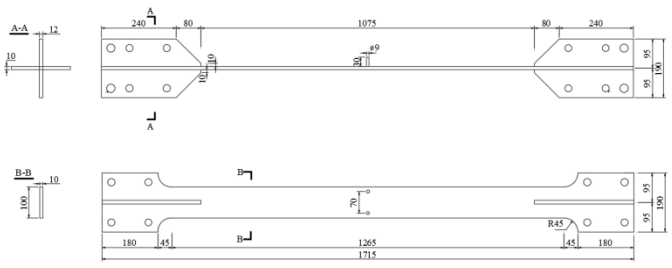

(b) Core member

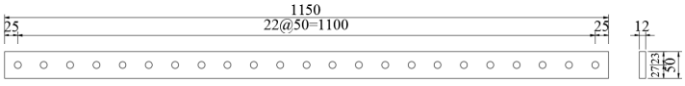

(c) Filler strip

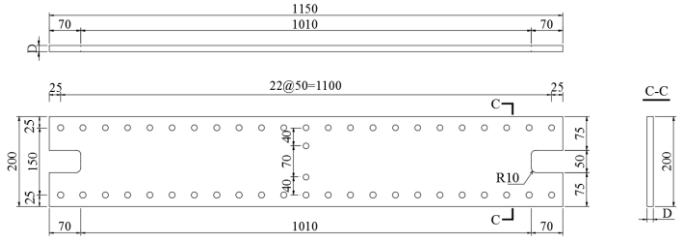

(d) Restraining plate

Fig. 10 Dimensions of the BRB specimens

Table 4
Factors of the BRB specimens

	D (mm)	d (mm)	ε_{nom}	v_l (mm/s)
BRB1-3	14	1	3%	0.1
BRB1-2	14	1	2%	0.1
BRB-2-3-A	14	2	3%	0.3
BRB-2-2-A	14	2	2%	0.6
BRB1.5-3	30	1.5	3%	0.3
BRB1.5-2	30	1.5	2%	0.3
BRB2-3	30	2	3%	0.3
BRB2-2	30	2	2%	0.3

Note: D is the thickness of the restraining plate; d is the clearance between the core member and the restraining plate; ε_{nom} is the nominal strain amplitude; v_l is the loading velocity of the test.

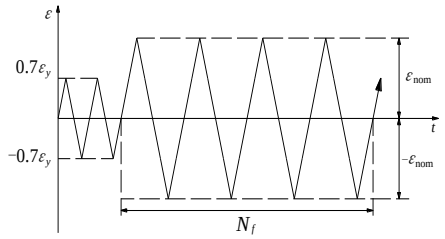

Fig. 11 Loading protocol

3.3 Testing setup

The specimens were tested in a quasi-static reversed loading test on the material testing system (MTS) shown in Fig. 12. The MTS is an electrohydraulic testing machine, whose load resisting capacity is ±1000 kN. The load value of the MTS actuator was collected using a force transducer embedded in the system. However, the displacement of the actuator is composed of the specimen deformation and the actuator elastic deformation. The specimen deformation includes not only the deformation of the yield segment but also the deformation of the connection and transition segment, which may cause the displacement value collected by the operating device of the MTS to exceed the actual deformation of the core member yield segment. To obtain the actual deformation of the core plate, four 100 mm-capacity LVDTs were vertically placed on the specimens, which were placed on the two ends of the core member, as shown in Fig. 12(a). A 50 mm-capacity LVDT was horizontally placed on the middle of a restraining plate to monitor the out-of-plane deformations of the BRB specimens. The axial force values and the displacement values were collected by the LVDTs and a TDS-530 data acquisition instrument. The ends of the BRB specimens were connected with the MTS by the connection plates and high-strength bolts, in which a pretension torsional moment of the high-strength bolts of 500 N.m is preloaded to minimize the probable slippage of the connections between the specimens and the MTS. The arrangement of the LVDTs and the connections between the specimens and the MTS are shown in Fig. 12(b) and Fig. 12(c), respectively.

The loading protocol of the experiment was divided into two stages: preloading stage and low-cycle reversed loading stage. In the preloading stage, two elastic deformation cycles with a strain amplitude of $0.7\varepsilon_y$ (ε_y is the yielding strain) were imposed on the specimens to assess the effectiveness of the loading system and TDS-530. The low-cycle reversed loading stage was conducted with a constant strain amplitude, in which the loading velocity ranged from 0.1-0.3 mm/s. The average strain amplitudes are listed in Table 4, and the loading protocol is shown in Fig. 11. The deformation of the core member yield segment is obtained using the LVDTs installed on the ends of the specimen, which are also used to control the MTS actuator.

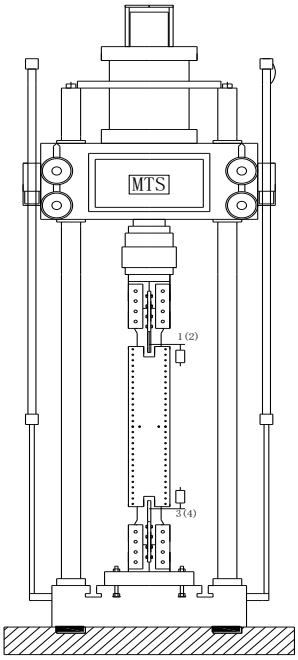

(a) Test machine

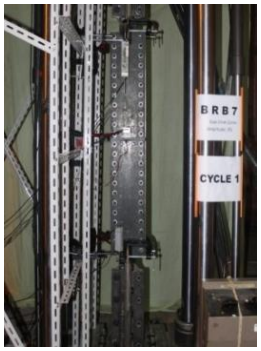

(b) LVDT arrangement

(c) Connection between the specimen and MTS

Fig. 12 Test setup

3.4 Testing results

First, the reversed loading tests on specimens BRB-1-3 and BRB-1-2 were conducted with a clearance value of 1 mm, with the thickness of the restraining plates equal to 14 mm. As mentioned in Section 3.3, two elastic deformation cycles were conducted to evaluate the validity of the MTS actuator. The two specimens were tested under nominal axial strain amplitudes of 3% and 2%, with the displacements of the actuator equal to 32.04 mm and 21.40 mm, respectively. The loading velocity was 0.1 mm/s. The test results revealed that the specimen BRB-1-3 fractured at the 16th cycle, while the failure position was at the middle of the core member, which was close to the stoppers (shown in Fig. 13(a)). Specimen BRB-1-2 fractured at the 27th cycle, and the failure position was one end of the yield segment, which is close to the stiffening rib weld, as shown in Fig. 13(b). As shown in Fig. 14(a) and (b), the specimens can perform stable hysteretic properties, although no buckling occurred on the restrainer (Fig. 13(a) and (b)). However, the cyclic number of specimen BRB-1-2 was considerably less than the reversed capacity of the Q235 steel material compared with the value in Table 2, which may be attributed to the existence of the weld on the core plate end, whose heat-affected zone can decrease its low-cycle fatigue capacity.

Second, specimens BRB-2-3A and BRB-2-2A were tested with a clearance value of 2 mm, and the thickness of the restraining plates was 14 mm. The constant strain amplitudes of the two specimens were 3% and 2%, respectively, while the loading velocity was 0.3 mm/s. The specimen BRB-2-3A fractured at the 9th cycle with significant global buckling, as shown in Fig. 13(c). The specimen BRB-2-2A fractured at the 20th cycle, with global buckling in some of the last cycles, as shown in Fig. 13(d). The low-cycle fatigue capacity of the two specimens significantly decreased compared with those of BRB-1-3 and BRB-1-2, while a significant tremble phenomenon was observed in the hysteretic curves shown in Fig. 14(c) and (d). According to the theoretical analysis in Section 2.1, the value of the contact force under compression exceeded the critical buckling load, which increased with the clearance. For the two specimens, the 14 mm-thick

(a) BRB1-3

(b) BRB1-2

(c) BRB2-3-A

(d) BRB2-2-A

(e) BRB1.5-3

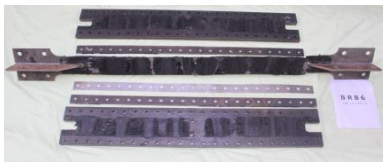

(f) BRB1.5-2

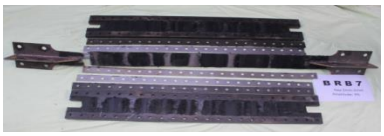

(g) BRB2-3

(h) BRB2-2

Fig. 13 Fracture mode of specimens

plates could not provide a sufficient amount of out-of-plane stiffness, which led to the global buckling. The tangent modulus of the specimen sharply decreased after the steel yielded, which further decreased the out-of-plane stiffness. The fracture occurred during the compression loading stage, while the fracture positions were on the end of the yield segment very close to the weld position, as shown in Fig. 14 (c) and (d).

As the amplification of the clearance may improve the out-of-plane stiffness demand of the restraining plates, the thickness of the restraining plate was increased to 30 mm, in which specimens BRB-1.5-3, BRB-1.5-2, BRB-2-3 and BRB-2-2 were tested. Specimens BRB-1.5-3 and BRB-1.5-2, whose clearance was 1.5 mm, were tested under strain amplitudes of 3% and 2%, respectively. Specimen BRB-1.5-3 fractured at the 10th cycle, while BRB-1.5-2 fractured at the 25th cycle. Specimens BRB-2-3 and BRB-2-2 were also tested with clearance values of 2.0 mm. BRB-2-3 fractured at the 7th cycle, while BRB-2-2 fractured at the 27th cycle. The fracture mode and hysteretic curves of the specimens are shown in Fig. 13(e-h) and Fig. 14(e-h). No global buckling occurred, which confirmed that the thickened restraining plates could provide a sufficient amount of out-of-plane stiffness. However, this finding also indicated that the cost of the specimens was increased, which decreased the cost performance in return. The low-cycle fatigue performance of these four specimens was also decreased compared with those of BRB-1-3 and BRB-1-2, which was similar to the specimens BRB-2-3A and BRB-2-2A, although the stiffness of the restrainer had been strengthened. These test results indicated that a large clearance cannot ensure the low-cycle fatigue performance.

The hysteretic curves shown in Figure 14 indicate that the 8 specimens can perform stable energy dissipation capacity, while their CPD capacities can substantially exceed the CPD demand stipulated by AISC2010 ($200\Delta_y$), as shown in Table 6. The unbonded material on the yield segment was worn at the contact position, which indicates that the unbonded material can be used to ascertain the crest and trough of the buckling wave. All specimens experienced multi-wave buckling, as shown in Fig. 13, while the analysis of the multi-wave buckling will be further conducted in Section 4.3.

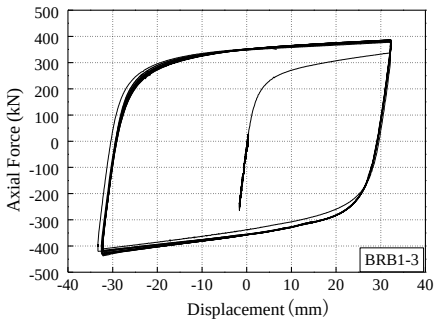

(a)

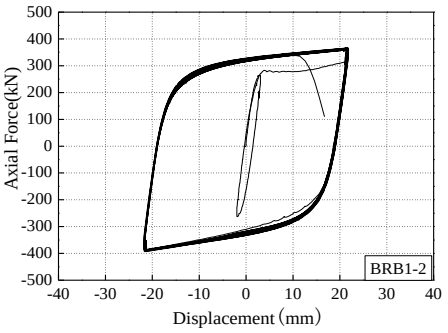

(b)

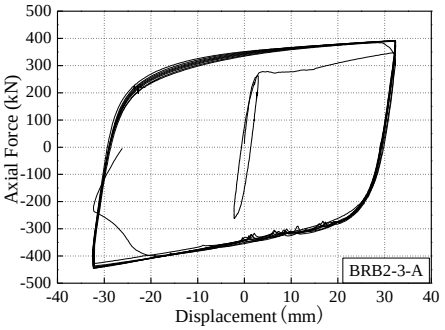

(c)

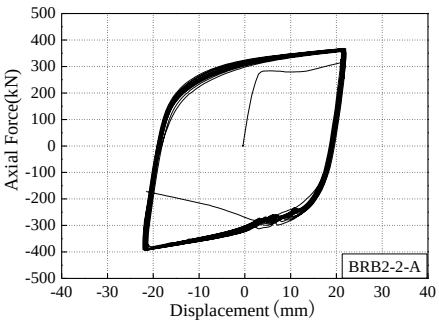

(d)

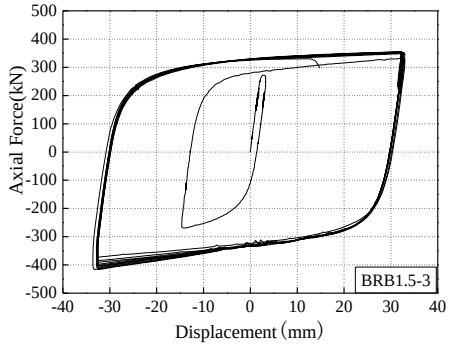

(e)

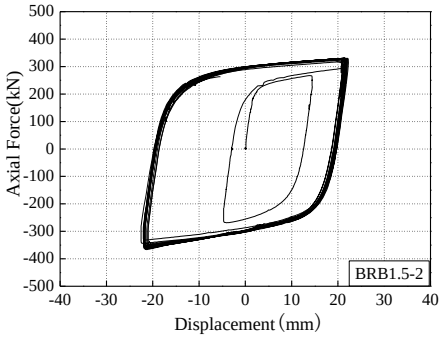

(f)

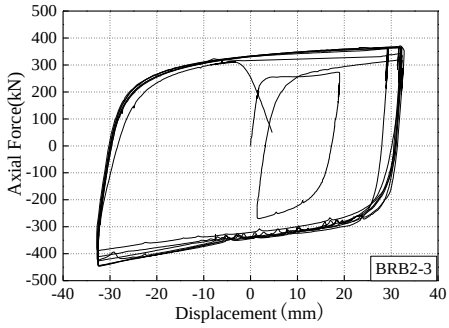

(g)

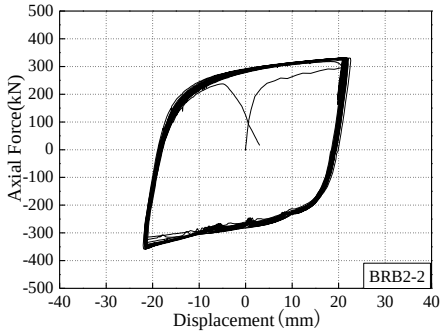

(h)

Fig. 14 Hysteretic curves of specimens

4. Influence of clearance on the performance of BRBs

4.1 Compression-strength adjustment factor

The compression-strength adjustment factor (β) of the specimens, which was obtained from the hysteretic curves, is listed in Table 5. Simultaneously, the numerical models of the BRB specimens were conducted using the method mentioned in Section 2.2; their compression-strength adjustment factors obtained via finite element analysis are also listed in Table 5. The variation trend of the compression-strength adjustment factor of the specimens is depicted in Fig. 15.

As shown in Table 5 and Fig. 15, the experimental values of the compression-strength adjust factor are consistent with the finite element analysis values because the ratio between the two values is almost distributed around the 45° line. The conclusion that the friction increases with the clearance can also be confirmed.

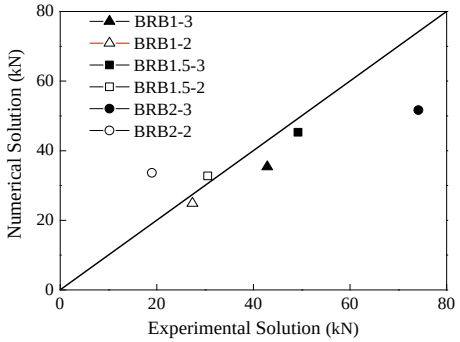

Fig. 15 Relationship of the compression-strength adjustment factor

Table 5
Compression-strength adjustment factor of specimens

	ε_{nom} (%)	d (mm)	EV (kN)	FV (kN)	β_E	β_F	β_C
BRB1-3	3	1	50.55	35.35	1.13	1.101	1.122
BRB1-2	2	1	25.75	24.86	1.07	1.072	1.105
BRB1.5-3	3	1.5	61.05	45.28	1.172	1.146	1.195
BRB1.5-2	2	1.5	35.85	32.74	1.108	1.109	1.150
BRB2-3	3	2	74.18	51.61	1.202	1.164	1.275
BRB2-2	2	2	26.10	33.63	1.078	1.112	1.200

Note: ε_{nom} is the nominal strain amplitude; d is the clearance between the core member and the restraining plate; EV is the experimental difference value of the compression force and tensile force, while FV is the finite element analysis difference value; β_E is the compression-strength adjustment factor obtained via experiment, while β_E and β_C are the factors obtained via numerical analysis and theoretical calculation, respectively.

4.2 Fracture of the specimens

The test phenomenon shown in Figure 14 indicates that only specimen BRB-1-3 fractured at the middle of the core member, while the other specimens fractured at the end of the yield segment. One important reason for these results is the influence of the weld, which causes a stress concentration and a decrease in the low-cycle fatigue performance due to the existence of a heat-affected zone. The influence of friction on this phenomenon should not be disregarded.

According to Section 2.1.2, the strain distribution of the sandwich BRBs with stoppers settled in the middle of the core member is not uniform, and the strain in the middle of the core member is less than the nominal strain amplitude, while the strain on the end of the yield segment is greater than the nominal strain amplitude. This trend is more significant with increasing clearance. When the clearance is relatively small, the friction is also small, and the distribution of the strain along the core member is relatively uniform. The fracture of the core member can occur at a random position. However, with increasing clearance, the strain of the yielding segment end is significantly greater than that in the middle, which shows that the low-cycle fatigue capacity of the member end is less than that in the middle and the low-cycle fatigue fracture is most likely occur at the end of the core member. The numerical result of specimen BRB-1-2 reveals that the strain on the core member end is 2.18%, while that on the middle is only 1.80%. This result indicates that the friction is a key factor that leads to a nonuniform strain distribution.

4.3 Low-cycle fatigue performance

The cycle number and CPD of the specimens (with the exception of BRB-2-3A and BRB-2-2A) are listed in Table 6. A comparison between the fatigue performance of the BRB specimens and the material specimens mentioned in Section 3.1 is also presented in the table.

It can be observed from Table 6 that the cycle number of specimens tested under a strain amplitude of 3% is less than that under a strain amplitude of 2%. This phenomenon is consistent with the conclusion of Section 3.1.2, which indicates that the low-cycle fatigue property of the specimens will decrease significantly with increasing strain amplitude.

As indicated in Table 6, the cycle number of specimen BRB-1-3 is 16, while that of the material 3% specimen is 19. The cycle numbers of the two tests are relatively consistent, while the BRB cycle number is slightly less than that of the material test specimen. First, the length of the BRB specimen is

substantially greater than that of the material test specimen, which may produce a larger amount of friction on the BRB. The nonuniform strain distribution is more substantial, which may cause a larger strain amplitude on the end. Furthermore, the ratio of the clearance to the core thickness in the BRB specimen (1/9.3) is relatively greater than that in the material specimen (1/20). The larger clearance-thickness ratio can cause a larger flexural moment and stress, which may decrease the low-cycle fatigue performance. However, the cycle number of specimen BRB-1-2 (27) is only 1/5 of that of the material 2% specimen (104), in which the low-cycle fatigue capacity failed to fulfill the requirement. Specimens BRB-1.5-2 and BRB-2-2 also remained within the range of 25-27 cycles, which was not less than that of BRB-1-2. The low-cycle fatigue capacity was not affected by the clearance due to the influence on the weld, which is responsible for the low-amplitude specimens (Usami et al. [26]). The heat-affected zone caused by the weld on the end of the core member may be a key factor that limits the low-cycle fatigue capacity, which indicates that the weld should be reduced or avoided if possible. Wang et al. [27, 28] proposed a type of partly welded BRB and obtained a larger cycle number. Xie et al. [11, 31] proposed a weld-free sandwich BRB, which can eliminate the effect on the weld, and obtained 147 reverse cycles of the core member under a strain amplitude of 2%.

Table 6
Fatigue performance of specimens

	d (mm)	ε_{nom} (%)	N_f	CPD	N_{fm}
BRB2-3	2	3	7	$641\Delta_y$	19
BRB1.5-3	1.5	3	10	$916\Delta_y$	19
BRB1-3	1	3	16	$1325\Delta_y$	19
BRB1.5-2	2	2	25	$1527\Delta_y$	104
BRB2-2	2	2	27	$1649\Delta_y$	104
BRB1-2	1	2	27	$1491\Delta_y$	104

Note: d is the clearance between the core member and restraining plate; ε_{nom} is the nominal strain amplitude; N_f is the cycle number of the BRB specimen; N_{fm} is the cycle number of material specimens.

A comparison of specimens BRB-1-3, BRB-1.5-3 and BRB-2-3 reveals that the low-cycle fatigue property decreases with the clearance, which causes a decrease in the cycle number. This finding is attributed to the notion that the flexural stress due to the buckling deformation of the specimen increases as the clearance increases. As mentioned in Section 3.4, the excessively low tangent modulus of the material may cause a further increase in the strain amplitude of the specimens and reduces the low-cycle fatigue capacity.

4.4 Fracture mechanism of sandwich BRBs

As indicated by the entire process of the reversed loading test, the BRB specimens primarily fractured on the yield segment end due to the weld and the friction. The weld on the end of the yielding segment cracked. Although the fracture did not immediately occur during the cycling, the cracks closed during the compression stage but extended when the specimens were under tension. The fracture therefore occurred after a certain number of cycles after the appearance of cracks.

The cracks of the weld on the core member end were caused by the stress concentration at the heat-affected zone of the weld, while the nonuniform strain distribution aggravated the development of cracks during the cyclic loading test. The actual effective area of the cross-section is smaller than the theoretical results due to cracks, which caused an increased stress and larger strain on the end of yielding segment. The cracks developed with the continued cycle loading, which aggravated the cross-section area, decreased and triggered brittle fracture in the weld heat-affected zone of the core member end.

Table 7
Buckling condition of BRB specimens

	P_E (kN)	P (kN)	P/P_E	n_e	n_f
BRB1-3	1.107	437.45	395.2	10	9
BRB1-2		393	355	9	9
BRB1.5-3		416.35	421	10	11
BRB1.5-2	0.989	366.45	370.5	10	10
BRB2-3		423.3	428	10	11
BRB2-2		356	360	9	9

Note: P_E is the critical buckling load of the specimens; P is the maximum load of the specimen; n_e is the quantity of buckling waves obtained via theoretical derivation, while n_f represents the test results.

Butyl rubber was used as unbonded material around the whole yielding segment to reduce the friction between the core member and the restrainer. The abrasion of the butyl rubber on the contact positions of the core member surface indicates the peaks and troughs of the buckling waves, as shown in Figure 14. Furthermore, the quantity of the buckling waves on the core member can be obtained by the number of abrasion positions. Note that this quantity only reflects the buckling in the last cycle of the tests.

The quantities of the buckling waves in the last cycle of the tests obtained by the experiment and the theoretical results are listed in Table 7. In Table 7, PE represents the critical buckling load of the specimens, which was obtained via Euler's formula, while the modulus is chosen as the tangent modulus. The test results are consistent with the theoretical results.

5. Clearance demand of the BRB

As mentioned in Section 2, the nonidentity of the value of the compression and tensile strength is an important factor that affects the strain distribution and the low-cycle fatigue performance of the core member, in which the friction is the main inducement. In this section, the analytic formula of the β value of the BRB is proposed; Poisson's effect is disregarded. The tensile force of the BRB can be expressed as

$$F_T = \sigma_\varepsilon \cdot A_e \tag{7}$$

where F_T is the tensile force of the BRB, σ_ε is the axial stress of the core member under strain ε, and A_e is the cross-section area of the core member. Only the core member bears an axial force, while the restrainer is free when the BRB is under tension.

The compression force of the BRB can be expressed as the sum of the compression force of the core member and the friction between the core member and the restrainer:

$$P = \sigma_\varepsilon \cdot A_e + f \tag{8}$$

where P is the axial force of the core member, σ_ε is the axial stress of the core member under strain ε, A_s is the cross-section area of the core member, and f is the friction between the core member and the restrainer, which can be obtained using Eq. (3) and (4).

Integrating Eq. (3), (7) and (8) into Eq. (1), the β value of the BRB can be expressed as

$$\beta = \frac{\sigma_\varepsilon A_e + \mu \cdot (2n)^2 \cdot \frac{Py_0}{\pi} \cdot \sqrt{\frac{P}{EI}}}{\sigma_\varepsilon A_e} \tag{9}$$

where n is the number of waves on one side of the core member, while the other symbols are identical to those in Eq. (1)-(8). The β value is proportional to the clearance between the core member and the restrainer, while the friction coefficient μ and the number of waves can also affect the β value. The β value is relative to the strain amplitude experienced by the core member, in which different strain amplitudes can directly cause different β values. The other factors are disregarded, and only friction is considered. The β values for the experimental specimens obtained via Eq. (9) are listed in Table 5. Comparing these calculated values β_C with the experimental values β_E and the numerical values β_F, Eq. (9) can be used to evaluate the β value.

As stipulated in AISC341-10, the β value should satisfy

$$\beta \le 1.3 \tag{10}$$

The clearance demand can be expressed by combining Eq. (9) and (10):

$$y_0 \le \frac{0.3F_T \cdot \pi\sqrt{EI}}{2n\mu P\sqrt{P}} = \frac{0.3\pi\sqrt{EI}}{2n\mu\sqrt{F_T} \cdot \beta^{\frac{3}{2}}} \tag{11}$$

where EI is the inertia moment of the core member, and the other symbols are listed in Eq. (7)-(10).

Considering that the core member predominantly yielded under compression, the tangent modulus E_t of the material is used for E in Eq. (11).

The clearance (y_0) demand between the core member and the restrainers of a certain BRB under a certain nominal axial strain amplitude and axial force can be obtained, where the friction coefficient μ is inversely proportional to the clearance demand. The unbonded material can release the β value, which is attributed to a decrease in the friction coefficient between the core member and the restrainer caused by the unbonded material.

Once a stricter β value limit is expected, Eq. (10) can be generalized as

$$\beta \le 1 + x \tag{12}$$

in which $0 \le x \le 0.3$.

Eq. (11) can also be generalized as

$$y_0 \le \frac{(\beta - 1) F_T \cdot \pi \sqrt{EI}}{2n\mu P \sqrt{P}} = \frac{(\beta - 1)\pi \sqrt{EI}}{2n\mu \sqrt{F_T} \cdot \beta^{\frac{3}{2}}} \tag{13}$$

The y_0 value upper limit of the BRB specimens in this paper is obtained using Eq. (11) and (13), in which the nominal strain amplitude is chosen to be 3% and 2%. The upper limit of the β value is chosen to be 1.3, 1.2 and 1.1. Simultaneously, the laying of the unbonded material is regarded as a variable in this analysis, in which the contribution of the unbonded material to the β value is verified. The friction coefficient between the core member and the restrainer is 0.3 without laying the unbonded material, while 0.1 is selected when the unbonded material is laid according to GB50017-2017 [29] and Jia et al. [30].

Table 8
y_0 demand of BRB specimens

β	Unbonding material	Friction coefficient	ε_{nom}=3%	ε_{nom}=2%
1.3	no	0.3	0.727	0.829
	lay	0.1	2.42	2.49
1.2	no	0.3	0.547	0.622
	lay	0.1	1.64	1.868
1.1	no	0.3	0.311	0.353
	lay	0.1	0.934	1.06

Note: ε_{nom} is the nominal strain amplitude of test specimens; "no" means no unbonding material laid on the specimen, while "lay" means that unbonding material is laid on the specimen.

Table 8 reveals that laying the unbonded material can effectively release the limit of y_0 between the core member and the restrainer. Considering the condition in which the nominal strain amplitude is 3% and the β value upper limit is 1.3 as an example, the y_0 upper limit is 0.727 mm if no unbonded material is laid, whereas 2.42 mm can be allowed when laying the unbonded material. Achieving a clearance demand less than 1 mm is difficult, while laying the unbonded material during the design of a BRB is feasible. The upper limit of y_0 is released with decreasing nominal strain amplitude, which can be observed from Table 8. Furthermore, a stricter β upper limit will cause a considerably stricter y_0 upper limit. Note that the upper limit of the y_0 value can make the β value satisfy the stipulation of AISC341-10, while a trend of the hysteretic curves in the compression stage is observed in the test specimens whose y_0 value is 2 mm, as shown in Figure 13(c), (d), (g) and (h). A similar phenomenon is also observed in Reference [28]. This phenomenon reveals that the clearance should be limited by the β value upper limit, and the hysteretic performance of the actual specimens should also be considered.

Poisson's effect of the core member should not be disregarded in the design because the cross-sectional area increases under compression and may fill the clearance. Once the reserved clearance is too thin, the restrainer may form a hoop effect on the core member, which can significantly improve the compressive strength of the BRB specimen. The specimen may not yield first, and the elastic strain of the main members may not be ensured in this condition, which may decrease the ductility of the whole structure. Furthermore, the restrainer may bear a large force, which may cause fracture. Thus, a minimum value for the clearance between the core member and the restrainer should be reserved.

Poisson's ratio is chosen to be 0.5 for the plastic condition, while the transverse strain can be obtained as

$$\varepsilon_t = v\varepsilon_v = 0.5\varepsilon_v \tag{14}$$

where ε_v is the axial strain of the core member, ε_h is the transverse strain, and v is Poisson's ratio.

The minimum clearance value of the in-plane direction can be defined as $d_{0,\,min}$:

$$d_{0,\min} = 0.5B\varepsilon_t = 0.25B\varepsilon_v \tag{15}$$

where B is the width of the core member.

Similarly, the minimum clearance value of the out-of-plane direction is defined as d_{min}:

$$d_{\min} = 0.25t\varepsilon_v \tag{16}$$

where t is the thickness of the core member.

The minimum clearance can be obtained from Eq. (14)-(16). The minimum clearance of the in-plane direction and out-of-plane direction of the specimens in this paper is 0.15 mm. In conclusion, the contribution of the unbonded material in limiting the β value should be considered, in which an upper limit of the clearance should be obtained by Eq. (11) or (13). Simultaneously, the clearance value should not be less than the minimum value obtained using Eq. (15) and (16). Furthermore, the stability of the hysteretic property of the specimens should also be considered. It is essential to mention that the analytical solution of this paper could be applied as a standard for sandwich BRBs, while it could also be used for BRBs whose yielding segments of the core member are manufactured from steel plates.

6. Conclusion

The influence of the clearance between the core member and the restrainer on the mechanical performance of BRBs is analyzed in this paper via experimental and numerical studies.

Six finite element models of BRBs with various clearances were conducted, and the multi-wave buckling of the BRB core members was analyzed. The strain distribution along the core member was not uniform due to the clearance effect. The results indicated that the core member buckles under compression when the load exceeds the critical buckling load and the core member is in contact with the restrainer due to the contact force between them. Additionally, the relative movement trend causes friction between them, which leads to a nonuniform strain distribution along the core member. This phenomenon causes the strain on the core member end to exceed the nominal value, while it is lower in the middle of the core member, which hinders expression of the low-cycle fatigue property of the specimen. When the friction increases with the amplification of the clearance, it causes an increase in the compression-strength adjustment factor (β) and aggravates the nonuniformity of the strain distribution on the core member. The low-cycle fatigue property of the specimen is significantly decreased.

Eight sandwich BRB specimens that were manufactured with different clearances were tested under reversed loading, in which the compression-strength adjustment factors, the CPDs, the energy dissipation capacity and the buckling characteristic were analyzed. The experimental results revealed a stable hysteretic property and energy dissipation capacity, which can satisfy the stipulated value of AISC2010. However, the compression-strength adjustment factor increased with the clearance, and the cycle number under the same strain amplitude decreased. Specimen BRB-1-3, whose nominal strain amplitude is 3% with a clearance value of 1 mm, can achieve a full low-cycle fatigue capacity. However, the low-cycle fatigue capacity of specimens with a clearance of 1.5 mm and 2 mm significantly decreased, which is in agreement with the theoretical derivation and numerical analysis. Conversely, the specimens with a nominal strain amplitude of 2% performed a relatively stable cycle number, which seemed to prevent the influence on the clearance. However, the cycle numbers of the BRB specimens were significantly less than those of the material specimens. The fracture positions were mostly concentrated on the end of the yielding segment of the core member because the weld heat-affected zone cracked during the reversed loading tests, which caused brittle failure of the specimens, while the low-cycle fatigue capacity of the material could not be fully displayed. Furthermore, the larger clearance signifies a higher restrainer stiffness demand, which may decrease the cost performance of the BRBs.

A formula for evaluating the compression-strength adjustment factor is deduced, which confirms that the calculated value is consistent with that of the experimental value and the numerical analysis results. The upper limit of the clearance is also proposed by considering the β value limit, while the lower limit can be restricted by considering Poisson's effect. The results also confirmed that the clearance between the core member and the restrainer

should be strictly limited in the design of the BRB for assuring the low-cycle fatigue performance, which should be limited according to the formula derivation and experimental results. The influence of the weld should be solved by reducing or eliminating the weld on the specimens, which can help the specimens achieve a low-cycle fatigue performance under minimal nominal strain amplitude. The analytical solution of this paper could be used in BRBs whose yielding segments of the core member are manufactured from steel plates.

References

[1] Usami T., Wang C. L. and Funayama J., "Developing high-performance aluminum alloy buckling-restrained braces based on series of low-cycle fatigue tests", Earthquake Engineering & Structural Dynamics, 41(4), 643-661, 2012.

[2] Tsai K.C., Hsiao P.C., Wang K.J.,Weng Y.T., Lin M.L., Lin K.C., Chen C.H., Lai J.W. and Lin S.L., "Pseudo-dynamic tests of a full-scale CFT/BRB frame—Part I: Specimen design, experiment and analysis", Earthquake Engineering & Structural Dynamics, 37(7), 1081-1098, 2008.

[3] Chou C.C. and Chen S.Y., "Subassemblage tests and finite element analyses of sandwich buckling-restrained braces", Engineering Structures, 32(8), 2108-2121, 2010.

[4] Vargas R. and Bruneau M., "Experimental response of buildings designed with metallic structural fuses. II", Journal of structural engineering, 135(4), 394-403, 2009.

[5] Usami T., Wang C. and Funayama J., "Low-cycle fatigue tests of a type of buckling restrained braces", Procedia Engineering, 14, 956-964, 2011.

[6] Feng Y.L., Wu J. and Meng S.P., "Elastic displacement spectrum-based design approach for buckling-restrained braced frames", Journal of Earthquake Engineering, 20(6), 841-860, 2016.

[7] Wu J., Liang R.J., Wang C.L. and Ge H.B., "Restrained buckling behavior of core component in buckling-restrained braces" International Journal of Advanced Steel Construction, 8(3), 212-225, 2012.

[8] Takeuchi T., Hajjar J.F., Matsui R, Nishimoto K. and Aiken I.D., "Effect of local buckling core plate restraint in buckling restrained braces", Engineering Structures, 44, 304-311, 2012.

[9] AISC A. "AISC 341-10, Seismic Provisions for Structural Steel Buildings", Chicago, IL: American Institute of Steel Construction, 2010.

[10] Uang C.M., Nakashima M. and Tsai K.C., "Research and application of buckling-restrained braced frames", International Journal of Steel Structures, 4(4), 301-313, 2004.

[11] Xie L.Q., Wu J. and Huang Q., "Experimental Study on Low-Cycle Fatigue Performance of Weld-Free Buckling-Restrained Braces", Journal of Earthquake Engineering, 22(8), 1392-1414, 2018.

[12] Jiang Z.Q., Dou C., Guo Y.L. and Zhang A.L., "Theoretical study on design methods for pinned assembled BRB with flat core", Engineering Structures, 133, 1-13, 2017.

[13] Wu B. and Mei Y., "Buckling mechanism of steel core of buckling-restrained braces", Journal of Constructional Steel Research, 107, 61-69, 2015.

[14] FEMA450 F. "NEHRP recommended provisions for seismic regulations for new buildings and other structures, Part 1: Provisions", Washington (DC, USA), BSSC, 2003.

[15] Black C.J., Makris N. and Aiken I.D., "Component testing, seismic evaluation and characterization of buckling-restrained braces", Journal of Structural Engineering, 130(6), 880-894, 2004.

[16] Wang C.L., Usami T., Funayama J. Imase F., "Low-cycle fatigue testing of extruded aluminium alloy buckling-restrained braces", Engineering Structures, 46, 294-301, 2013.

[17] Jia M.M., Yu X.H., Lu D.G. and Lu B.B. "Experimental research of assembled buckling-restrained braces wrapped with carbon or basalt fiber", Journal of Constructional Steel Research, 131, 144-161, 2017.

[18] Guo Y.L., Fu P.P., Zhou P. and Tong J.Z. "Elastic buckling and load resistance of a single cross-arm pre-tensioned cable stayed buckling-restrained brace", Engineering Structures, 126, 516-530, 2016.

[19] Guo Y.L., Zhou P., Bradford M.A., Pi Y.L., Tong J.Z. and Fu P.P., "Theoretical and numerical studies of elastic buckling and load resistance of double cross-arm pre-tensioned cable stayed buckling-restrained braces", Engineering Structures, 153, 674-699, 2017.

[20] Sabelli R., "Research on improving the design and analysis of earthquake-resistant steel-braced frames", EERI, 2001.

[21] Iwata M., Kato T. and Wada A., "Performance evaluation of buckling-restrained braces in damage-controlled structures", Behavior of steel structures in seismic areas: STESSA, 37-43, 2003.

[22] Usami T., Kasai A. and Kato M., "Behavior of buckling-restrained brace members", Behavior of Steel Structures in Seismic Areas, Proc., 4th Int. Conf. STESSA 2003. Naples, Italy, 211-216, 2003.

[23] Lin P.C., Tsai K.C., Chang C.A., Hsiao Y.Y. and Wu A.C., "Seismic design and testing of buckling-restrained braces with a thin profile", Earthquake Engineering and Structural Dynamics, 45(3), 339-358, 2016.

[24] Matsui R. and Takeuchi T., "Cumulative Deformation Capacity of Buckling Restrained Braces Taking Local Buckling of Core Plates into Account", Proc. 15th World Conference on Earthquake Engineering (Lisbon), 2012.

[25] Takeuchi T. and Wada A., "Buckling-Restrained Braces and Applications", JSSI, 2017

[26] Usami T., Sato T. and Kasai A., "Developing high-performance buckling-restrained braces", Journal of Structural Engineering, 55, 719-729, 2009.

[27] Wang C.L., Usami T. and Funayama J., "Evaluating the influence of stoppers on the low-cycle fatigue properties of high-performance buckling-restrained braces", Engineering Structures, 41, 167-176, 2012.

[28] Wang C.L., Li T., Chen Q. and Wu J., "Experimental and theoretical studies on plastic torsional buckling of steel buckling-restrained braces", Advances in Structural Engineering, 17(6), 871-880, 2014.

[29] GB 50017-2017, Code for design of steel structure, Ministry of Housing and Urban-Rural Development of the People's Republic of China, Beijing, 2017. (in Chinese)

[30] Jia M.M., Zhang S.M. and Lu D.G., "Stability behavior and ductility performance analysis of buckling restrained braces", Journal of Building Structures (Supplementary Issue 2), 76-81, 2010. (in Chinese)

[31] Xie L.Q., Wu J., Huang Q. and Tong C., "Analysis of the Seismic Demand of High-Performance Buckling-Restrained Braces under a Strong Earthquake and its Aftershocks", Advances in Civil Engineering, 1482736, 2019.

Acknowledgments

The authors would like to acknowledge financial support from the National Natural Science Foundation of China (51978165), the China National Key Research and Development Program (2016YFC0701403) and the Priority Academic Program Development of Jiangsu Higher Education Institutions (PAPD).